# 2011 SCEC ANNUAL REPORT

## 1. SUMMARY REPORT OF MAJOR FINDINGS IN SCEC3

Our cumulative SCEC3 findings, summarized below, have been supported by SCEC Proposals 11080 (2011), 09141 (2009), and 08052 (2008) (PI Smith-Konter). Five primary findings have resulted from this work, and form the basis of several avenues of future research:

1) Modeled Coulomb stress accumulation rates of the San Andreas Fault System range from 0.5-7 MPa/100 years, vary as a function of fault locking depth, slip rate, and fault geometry, and are inversely proportional to earthquake recurrence intervals (20-500 years). [*Smith-Konter and Sandwell*, 2009]

2) Calculations of accumulated stress over several earthquake cycles are consistent with coseismic stress drops of ~ 3-8 MPa, however such calculations depend largely on the rupture history of the fault [e.g., *Grant and Lettis*, 2002; *Weldon et al.*, 2004] over the past few thousand years. [*Smith-Konter and Sandwell*, 2009]

3) Stress accumulation rate uncertainties, derived from a range of geodetically- and seismically-derived locking depth estimates, are roughly +3/-0.5 MPa/100 years; uncertainties derived from realistic slip rate variations are roughly +1/-0.5 MPa/100 years. Uncertainties in stress accumulation can range from 1-5 MPa for various slip history scenarios based on updated paleoseismic earthquake chronologies, emphasizing the need for a comprehensive and conclusive paleoseismic database. [*Smith-Konter et al*., in preparation]

4) There is generally good agreement between seismogenic thickness and geodetic locking depth along the San Andreas Fault System in southern California, with 9 out of the 12 fault segments analyzed agreeing to within 2 km. However, three segments (Imperial, Coyote Creek, and Borrego) have significant discrepancies, with seismic estimates that are well outside the error bounds of the geodetic locking depths. In these cases, the geodetically-inferred locking depths are much shallower than the seismogenic depths, which may be due to complications from shallow creep. [*Smith-Konter et al*., 2011]

5) Dislocation models generally produce high strain rates near faults when compared to alternative methods (i.e. isotropic gridding of sparse PBO GPS data (10-15 km spacing) results in strain rates 5-8 times lower). Variations in dislocation model strain rates are due to differences in applied slip rates and locking depths. The greatest differences occur within 15 km of major faults. [*Smith-Konter et al*., 2010; *Wei et al*., 2010; *Tong et al*., in preparation]

## 2. TECHNICAL REPORT FOR 2011 SCEC PROPOSAL 11080

**Investigating along-strike depth variations of seismicity along the San Andreas Fault System to better resolve geodetic locking depths**

SUBMITTED PROPOSALS RELATED TO THIS PROJECT:

NSF EarthScope ($200,938) 1/1/12 - 12/31/14; *Collaborative research: Strain rate and moment accumulation rate along the San Andreas Fault System from InSAR and GPS;* PI B. Smith-Konter; Co-PI D. Sandwell (UC San Diego)

Southern California Earthquake Center ($18,974) 2/1/12 - 1/31/13; *Investigating absolute stress in Southern California constrained by earthquake focal mechanisms and models of stress contributions from topography and fault loading*; PI B. Smith-Konter; Co-PIs K. Luttrell (USGS) and D. Sandwell (UC San Diego)

PUBLICATIONS AND ABSTRACTS RELATED TO THIS PROJECT:

Smith-Konter, B., D.T. Sandwell, and P. Shearer (2011), Locking depths estimated from geodesy and seismology along the San Andreas Fault System: Implications for seismic moment release, *J. Geophys. Res.*, 116, B06401, doi:10.1029/2010JB008117.

Smith-Konter, B. (2012), Stress uncertainties of the San Andreas Fault System from 4-D deformation modeling, submitted to the *2012 Seismol. Soc. Amer. Meeting.*

Tong, X., D. Sandwell, and B. Smith-Konter (2012), High resolution interseismic crustal velocity model of the San Andreas fault from GPS and InSAR, submitted to the *2012 Seismol. Soc. Amer. Meeting.*

Smith-Konter, B. and C. Del Pardo (2011), EarthScope imaging of 4D stress evolution of the San Andreas Fault System, *Abstract G53C-03 presented at the 2011 Fall Meeting*, AGU, San Francisco, Calif., 5-9 Dec.

Tong, X., D. Sandwell, and B. Smith-Konter (2011), High resolution interseismic velocity model of the San Andreas fault from GPS and InSAR, *Abstract G41A-0723 presented at the 2011 Fall Meeting*, AGU, San Francisco, Calif., 5-9 Dec.

Del Pardo, C. and B. Smith-Konter (2011), Investigating variations in strain rate of the San Andreas Fault System due to dipping fault geometry resolved by geodetic and seismicity data, *Abstract G41A-0722 presented at the 2011 Fall Meeting*, AGU, San Francisco, Calif., 5-9 Dec.

Tong, X., D.T. Sandwell, and B. Smith-Konter (2011), High resolution interseismic crustal velocity model of the San Andreas Fault System from GPS and InSAR, *SCEC Annual Meeting*, Palm Springs, CA.

Luttrell, K., D.T. Sandwell, and B. Smith-Konter (2011), Absolute stress in southern California constrained by earthquake focal mechanisms and models of stress contributions from topography and fault loading, *SCEC Annual Meeting*, Palm Springs, CA.

Del Pardo, C., B. Smith-Konter, D. Sandwell, P. Shearer, and Y. Zeng (2011), Investigating along-strike depth variations of seismicity in the San Andreas Fault System to better resolve geodetic locking depths, *SCEC Annual Meeting*, Palm Springs, CA

Smith-Konter, B. and C. Del Pardo (2011), 3D volume visualizations of stress accumulation rates of the San Andreas Fault System, *2011 EarthScope National Meeting*.

Tong, X., D.T. Sandwell, and B. Smith-Konter (2011), High resolution interseismic crustal velocity model of the San Andreas Fault System from GPS, InSAR, and a dislocation model, *2011 EarthScope National Meeting*.

Sandwell, D., M. Wei, and B. Smith-Konter (2011), Integrating GPS and InSAR to Resolve Strain Rates Along the San Andreas Fault System: Contributions from ALOS-1/2 and DESDynI, *2011 IGARRS Meeting*.

MANUSCRIPTS IN PREPARATION RELATED TO THIS PROJECT:

Smith-Konter, B., C. Del Pardo, T. Solis, and D.T. Sandwell, Stress uncertainties of the San Andreas Fault System, *to be submitted to J. Geophys. Res.*

Tong, X., D. Sandwell, and B. Smith-Konter, High-resolution interseismic velocity data along the San Andreas fault from GPS and InSAR, to be submitted to *J. Geophys. Res*.

---

The primary objective of this project is to investigate depth variations of the seismogenic zone beneath the San Andreas Fault System (SAFS) using both seismic and geodetic methods. Seismic hazard models of the SAFS (i.e. the UCERF3 model) rely on an accurate representation of fault depths to properly estimate the earthquake potential of active faults. Such hazard models typically utilize quantities like strain rate or moment accumulation rate to evaluate earthquake potential, both of which depend largely on slip rate and fault depth [e.g., *Meade and Hager*, 2005b; *Parsons*, 2006; *WGCEP*, 2007; *Freed et al*., 2007; *Stein*, 2008; *Smith-Konter and Sandwell*, 2009]. Furthermore, relocated earthquake hypocenters in southern California show that the depth above which 99% of the moment release of background seismicity occurs provides a reasonable estimate of the maximum depth of rupture in moderate to large earthquakes [*Nazareth and Hauksson,* 2004]. Thus accurate estimates of maximum fault depth are fundamental in forecasting the magnitude of future earthquakes.

Both geodetic and seismic estimates of depth used here are typically an along-strike average of the data sampled for each predefined fault segment. How realistic is this assumption? In particular, as geodetic depth estimates are dependent upon model fault geometry and segmentation resolution, they require a fairly complicated segmentation scheme to provide sufficient along-strike resolution to address realistic depth variations. Hence a resulting goal of this project is to tune our fault model segmentation using variations in seismicity depths from comprehensive earthquake hypocenter catalogs.

For this project, we established three primary research tasks:

- *Task 1: Evaluation of SAFS segmentation using along-strike seismicity depth variations*
- *Task 2: Determination of new fault locking depths from GPS inversion*
- *Task 3: Comparison of community velocity and strain maps (provided by Y. Zeng)*

We are pleased to report that we were able to complete all three of these tasks in a reasonable time frame and have presented the results at both SCEC and AGU meetings and in a related manuscript [*Smith-Konter et al*., 2011]. Three primary findings have

resulted from this work, described in further detail in the following pages, which form the basis of future research:

1) Using a simplified fault segmentation for the southern SAFS, there is generally good agreement between seismogenic thickness and geodetic locking depth, with 9 out of the 12 fault segments analyzed agreeing to within 2 km (Figure 1) [S*mith-Konter et al*., 2011]. A regression analysis of geodetic depth versus seismic depth yields a standard deviation of 4.16 km. However, three segments (Imperial, Coyote Creek, and Borrego) have significant discrepancies, with seismic estimates that are well outside the error bounds of the geodetic locking depths. In these cases, the geodetically inferred locking depths are much shallower than the seismogenic depths.
2) Along the southern SAFS, 13 of the 20 segments considered in this study require additional sub-segmentation to properly represent along-strike seismicity variations. The role of across-fault seismicity width was also investigated, suggesting that seismic depths typically increase by 1-3% when the seismic window is widened (10 km vs. 5 km).
3) Comparisons of our strain rate model with other dislocation models illustrates that some regions of the SAFS accommodate strain at rates higher than suggested by alternative methods (i.e., isotropic gridding of sparse PBO GPS data (10 – 15 km spacing) results in strain rates 5 – 8 times lower). Variations in dislocation model strain rates are due to differences in applied slip rates and locking depths. The greatest differences occur within 15 km of major faults.

In this study, we re-evaluated the along-strike segmentation of the San Andreas, San Jacinto, and Elsinore faults in southern California using variations in depths of seismicity from the earthquake hypocenter catalog of *Lin et al*. [2007]. This catalogue utilizes waveform cross-correlation and a new 3D velocity model for southern California to relocate 400,000 earthquakes between 1981 and 2005. We use the UCERF3 fault segmentation as a first-order model of major fault segments and examined seismicity profiles as a function of depth for each segment. To achieve robust depth estimates that are insensitive to occasional stray earthquake locations at large depth, we assign a cutoff percentile depth at 90%, 95%, and 99% to define the maximum depths of seismicity. For segments that have significant along-strike variations in maximum depth of seismicity, or gaps in seismicity, we attempt to refine the fault segmentation to accommodate these observed variations. Segment definitions were qualitatively assigned based on observed seismicity breaks, both from map view and from each along-strike profile.

In total, 20 total segments were investigated in this study. Of these, we find that 13 segments require additional sub-segmentation to properly represent along-strike seismicity variations [*Del Pardo et al*., 2011 SCEC Poster A-054]. Segments that do not need additional sub-segmentation are Palm Springs, Coyote Creek, Superstition Hills North, San Jacinto Valley, Borrego, San Jacinto Mountains, and Cholame. Alternatively, segments for which further sub-segmentation is suggested are Cerro Prieto, Imperial (southern and northern sections), Brawley, Coachella Valley, San Bernardino Mountains, Superstition Hills South, Anza, Mojave, Carrizo, and Parkfield. A summary of these results for two example segments (Imperial and Coachella) is provided in Figure 2.

For the Coachella segment, we initially estimated an 11.6 km depth derived from a 99% seismicity cutoff depth. Further inspection of seismicity along-strike prompted us to

sub-divide this segment into 3 pieces (a, b, and c) (Figure 2). Using this revised sub-segmentation, we find that segment Coachella-a yields a seismic depth (99% seismicity cutoff) of 13.4 km, Coachella-b a depth of 15.4 km, and Coachella-c a depth of 10.9 km. Coachella-b demonstrates the deepest distribution of seismicity, although the number of earthquakes in this segment is very small (197); Coachella-c prefers the (relative) shallowest depth of seismicity, as there are a significant number of earthquakes that cluster at a depth range of 5-10 km. The geodetic depth that we determine, using the full Coachella segment length, is 11.5 km. This depth is most closely aligned with the depth of seismicity determined from the Coachella-c sub-segment, however the ensemble average of the seismicity data for this segment provided a very good match to begin with (11.6 km). We also note an obvious eastward offset of the seismicity from the mapped fault trace along the Coachella-a and Coachella-b segments. Motivated by this observation, we have begun to explore this offset in the context of a dipping geometry in an updated version of our semi-analytic crustal deformation modeling code (described next, now capable of simulating dipping fault traces).

Evidence of depth variation is also observed along the Imperial segment (Figure 2), where seismicity along the northern section appears to cluster at a deeper depth than along the southern section. For the southern Imperial segment, geodetically-determined depths appear to track mid-depth clusters of seismicity, revealing how geodetic methods only estimate the thickness of the locked zone. For example, maximum seismicity depths (99% seismicity cutoff) of the Imperial fault suggest a seismogenic thickness of ~15 km, while geodetic measurements place the fault locking depth much shallower, at 5.5 km, where a significant portion of the seismicity is also located. Revised seismicity depths using a refined segmentation (Imperial a, b, c) provide a range of depth estimates (12.3, 19.9 and 18.4 km, respectively; 99% seismicity cutoff). Thus we find a reduction of seismicity depths for the northernmost section of the southern Imperial fault, however this depth remains significantly larger than the geodetic estimate. The Imperial fault is known to exhibit fairly complex slip behavior with associated creep and perhaps cannot be accurately geodetically modeled as a single fault segment that is simply locked at depth [*Lyons et al*., 2002; *Wdowinski*, 2009].

In this study we also test the sensitivity of seismic depths to the width of the seismicity window surrounding a fault segment. Previous work suggests that the inclusion of earthquakes within 5 km of each fault trace provides a reasonable representation of the active fault zone. As a test case, we used the seismicity distribution of the Mojave segment, spanning seismicity window widths of 5 and 10 km. We find an overall increase in calculated seismic depth by 1-3%, depending on the cutoff percentile depth of seismicity (90% depth, 2.3% increase; 95% depth, 1.4% increase, and 99% depth, 3.3% increase). Thus when the seismic window size is doubled (10 km vs. 5 km), we observe a slight decrease in the discrepancy between seismic (14.9 vs. 14.4 km, respectively) and geodetic locking depth (16.8 km) along the Mojave segment. Similar behavior is observed along the other segments.

Using seismicity depth variations as a guide for fault segmentation, we re-calculated geodetic locking depths for the SAFS. As an additional feature of this work, we also employed a new component of our 3-D semi-analytic crustal deformation model [*Smith and Sandwell*, 2004; *Del Pardo et al*., 2011, AGU poster G41A-0722] that includes dipping fault kinematics approximated by numerical integration. For this task, we used

the unified GPS velocity field compiled by T. Herring and adopted geologic slip rate estimates primarily defined by the UCERF3 modeling community. A rigorous inversion of fault locking depths was used to tune the model, in which we identified improved locking depth estimates and prescribed dip geometries along the Coachella, Palm Springs, Mojave, and Carrizo segments. From these results we calculated a revised strain rate field of the SAFS. The incorporation of dipping fault geometry and revised fault depths significantly modified strain rate magnitudes (~ -200/+800 nanostrain/yr variation) and peak strain rate locations (horizontal shift) within the fault zone (Figure 3). Shallow locking depths yield higher strain rates than deep locking depths. The highest strain rates are evident along the Cerro Prieto (average $d$ = 5 km), Imperial (average $d$ = 6 km), Creeping (average $d$ = 2 km), and Calaveras (average $d$ = 1 km) segments.

Lastly, we extended a previous investigation of strain rate maps of California, led by D. Sandwell [*Sandwell et al*., 2010; *Smith-Konter et al*., 2010]. In collaboration with Y. Zeng (USGS), we compared strain rate results of both our updated dipping fault model (Smith-Konter) with Zeng's modeling methods. The Zeng model was developed by computing an inverse solution for fault slip rates in California using a fault-based model developed from the UCERF3 fault geometry and an updated GPS velocity model for the western US from T. Herring. The model was then used to simulate the strain rate distribution for California and its neighbors analytically using the method of *Okada* [1992]. Locking depths are defined by seismicity and a dipping fault geometry is included for all applicable faults. Residual strain rates based on the difference between the observed GPS velocities and the fault model predictions were calculated for all the GPS stations around California. Residual strain rates were then interpolated to a uniform grid using a modified approach of *Shen et al*. [1996]. This approach uses an azimuthal weighting scheme based on the area of the Voronoi cells determined for those GPS stations in addition to the Gaussian distance decay function and the GPS velocity error weighting. The final estimate of strain rate for the region was obtained by combining the predicted strain rate map and the interpolated residual strain rate map.

Previous comparisons of strain rate estimates from dislocation models [*SCEC UCERF3 Workshop Report*, 2010] have suggested that some regions of the SAFS accommodate strain at rates higher than suggested by alternative methods (i.e., isotropic gridding of sparse PBO GPS data at 10 – 15 km spacing results in strain rates 5 – 8 times lower). For this study, however, we directly compare two dislocation model approaches (Smith-Konter and Zeng) (Figure 3). We find that while these results have similar strain rate features over the entire plate boundary, significant differences are observed, due to variations in applied slip rates and locking depths. The greatest differences occur within 15 km of major faults. Regions of significant disagreement are highlighted along the Parkfield segment, where the Smith-Konter model estimates ~3000 nanostrain/yr and the Zeng model estimates < 200 nanostrain/yr. These differences are due to variations in the depth of shallow creep. The Zeng model assigns a locking depth between 8 and 15 km, but also permits shallow creep at depths above 5 km. The Smith-Konter model assigns a locking depth of 12 km with no shallow creep. Moreover, accurate estimates of strain accumulation rates are essential for understanding the earthquake cycle and future work will include additional tuning of our model using dense campaign GPS profiles and L-band radar interferometry [i.e., *Tong et al*., 2011].

## REFERENCES

Del Pardo, C. and B. Smith-Konter (2011), Investigating variations in strain rate of the San Andreas Fault System due to dipping fault geometry resolved by geodetic and seismicity data, *Abstract G41A-0722 presented at the 2011 Fall Meeting*, AGU, San Francisco, Calif., 5-9 Dec.

Del Pardo, C., B. Smith-Konter, D. Sandwell, P. Shearer, and Y. Zeng (2011), Investigating along-strike depth variations of seismicity in the San Andreas Fault System to better resolve geodetic locking depths, *SCEC Annual Meeting*, Palm Springs, CA

Lin, G., P. M. Shearer, and E. Hauksson (2007), Applying a three-dimensional velocity model, waveform cross correlation, and cluster analysis to locate southern California seismicity from 1981 to 2005, *J. Geophys. Res*., 112, B12309, doi:10.1029/2007JB004986.

Lyons, S., Y. Bock, and D. T. Sandwell (2002), Creep along the Imperial fault, Southern California, from GPS measurements, J. Geophys. Res., 107(B10), 2249, doi:10.1029/2001JB000763.

Meade, B.J., and B.H. Hager (2005), Spatial localization of moment deficits in southern California, *J. Geophys. Res*., 110, doi:10.1029/2004JB003331.

Nazareth, J. J., and E. Hauksson (2004), The seismogenic thickness of the southern California crust, *Bull. Seismol. Soc. Am*., 94, 940-960.

Okada, Y. (1992), Internal deformation due to shear and tensile faults in a half- space, *Bull. Seismol. Soc. Am*., 82, 1018–1040.

Parsons, T. (2006), Tectonic stressing in California modeled from GPS observations, *J. Geophys. Res*. 111, doi:10.1029/2005JB003946.

Sandwell, D., T. Becker, P. Bird, J. Bormann, A. Freed, M. Hackl, B. Meade, W. Holt, B. Hooks, S. Kedar, C. Kreemer, R. McCaffrey, T. Parsons, F. Pollitz, Z-K. Shen, B. Smith-Konter, C. Tape, and Y. Zeng (2010), Comparison of 16 strain rate maps for southern California, *2010 SCEC Annual Meeting* poster 1-125.

SCEC UCERF workshop report: http://www.scec.org/workshops/2010/gpsucerf3/Report_on_2010_-SCEC_GPS_UCERF3_Workshop_v2.pdf

Smith, B., and D. T. Sandwell (2004), A 3-D semi-analytic viscoelastic model for time-dependent analysis of the earthquake cycle, *J. Geophys. Res*., doi:10.1029/2004JB003185.

Smith-Konter, B., and D. T. Sandwell (2009), Stress evolution of the San Andreas Fault System: Recurrence interval versus locking depth, *Geophys. Res. Lett*., 36, doi: 10.1029/2009GL037235.

Smith-Konter, B., D. Sandwell, and M. Wei (2010a), Integrating GPS and InSAR to resolve stressing rates of the SAF System, *EarthScope inSights Newsletter*, Summer 2010.

Smith-Konter, B., D.T. Sandwell, and P. Shearer (2011), Locking depths estimated from geodesy and seismology along the San Andreas Fault System: Implications for seismic

moment release, *J. Geophys. Res.*, 116, B06401, doi:10.1029/2010JB008117.

Stein, R.S. (2008), Appendix D: Earthquake Rate Model 2 of the 2007 Working Group for California Earthquake Probabilities, Magnitude-Area Relationships, *U.S. Geol. Surv. Open File Rep*., 2007-1437D.

Tong, X., D. Sandwell, and B. Smith-Konter (2011), High resolution interseismic velocity model of the San Andreas fault from GPS and InSAR, *Abstract G41A-0723 presented at the 2011 Fall Meeting*, AGU, San Francisco, Calif., 5-9 Dec.

Wdowinski, S. (2009), Deep creep as a cause for the excess seismicity along the San Jacinto fault, *Nature Geosci*., 2, doi:10.1038/NGEO684.

Working Group on California Earthquake Probabilities (WGCEP) (2007), The Uniform California Earthquake Rupture Forecast, Version 2 (UCERF 2), *U.S. Geol. Surv. Open File Rep*., 2007-1473.

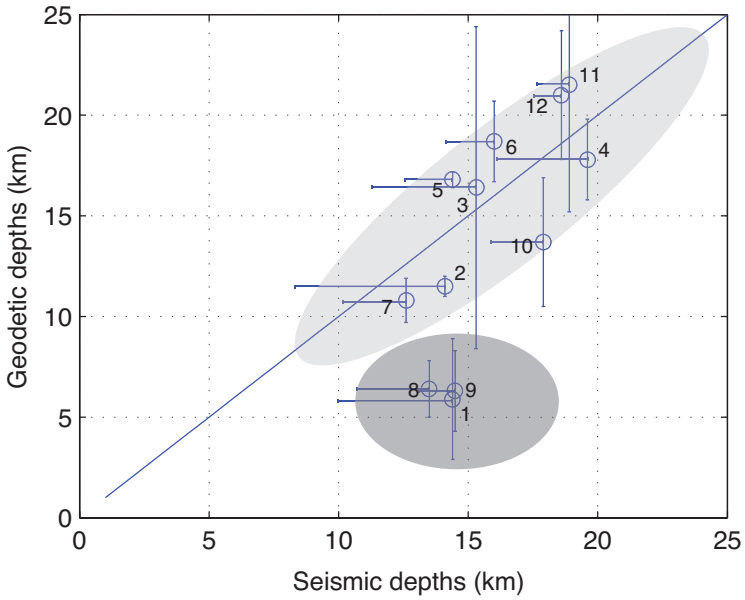


**Figure 1.** Comparison of seismogenic thickness (depths) estimated by LSH07 (99% seismicity cutoff depth, horizontal axis) and geodetic locking depths (vertical axis). Uncertainty estimates in geodetic depths and seismogenic depths (approximated from 90–99% seismicity cutoff depth estimates) are also plotted. Number labels correspond to segment numbers in Table 1 of *Smith-Konter et al.* [2011]. The light shaded oval represents data that cluster around the 1:1 match in depths, represented by the diagonal line. The dark shaded circle represents outliers (Imperial, Coyote Creek and Borrego) where seismicity suggests much deeper fault locking depths than geodesy.

**Figure 2. (next page)** Seismicity and depth estimates for Coachella and Imperial segments. For each segment panel, seismicity is presented for the entire segment in map view (upper left corner) and along strike as a function of depth (lower left corner). Results for this study's estimates of additional sub-segmentation are also presented (upper right corner). A table summarizing the depth estimates as a function of % of maximum seismicity depth is also provided for each segment.

## Coachella Valley

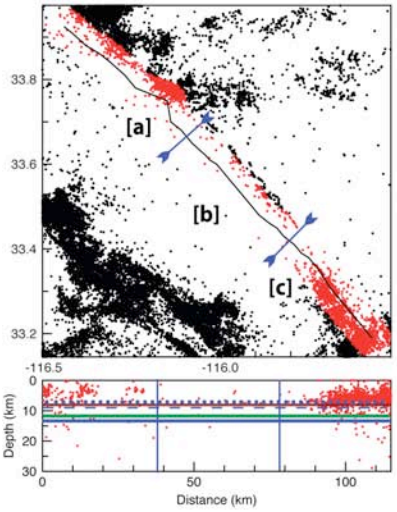


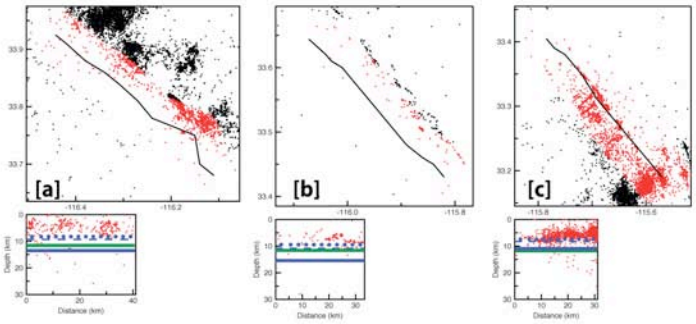


| Segment Number | Geodetic Depth (km) | Seismic Depth (km) 90% | 95% | 99% | Number of Earthquakes |
|---|---|---|---|---|---|
| 4 | 11.5 | 7.8 | 8.3 | 11.6 | 6666 |
| a | | 8.2 | 8.7 | 13.4 | 1637 |
| b | | 9.4 | 10.6 | 15.4 | 197 |
| c | | 7.4 | 7.9 | 10.9 | 4833 |

## Imperial South

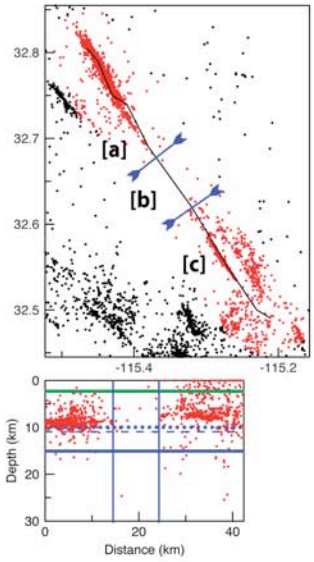


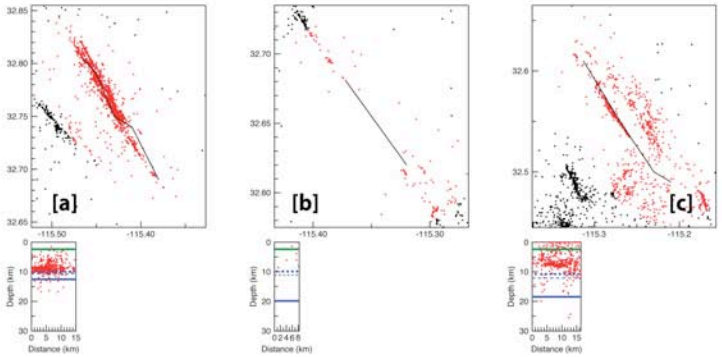


| Segment Number | Geodetic Depth (km) | Seismic Depth (km) 90% | 95% | 99% | Number of Earthquakes |
|---|---|---|---|---|---|
| 1 | 5.5 | 10.0 | 10.8 | 15.1 | 2702 |
| a | | 9.9 | 10.1 | 12.3 | 1810 |
| b | | 9.9 | 11.1 | 19.9 | 130 |
| c | | 10.9 | 11.6 | 18.4 | 891 |

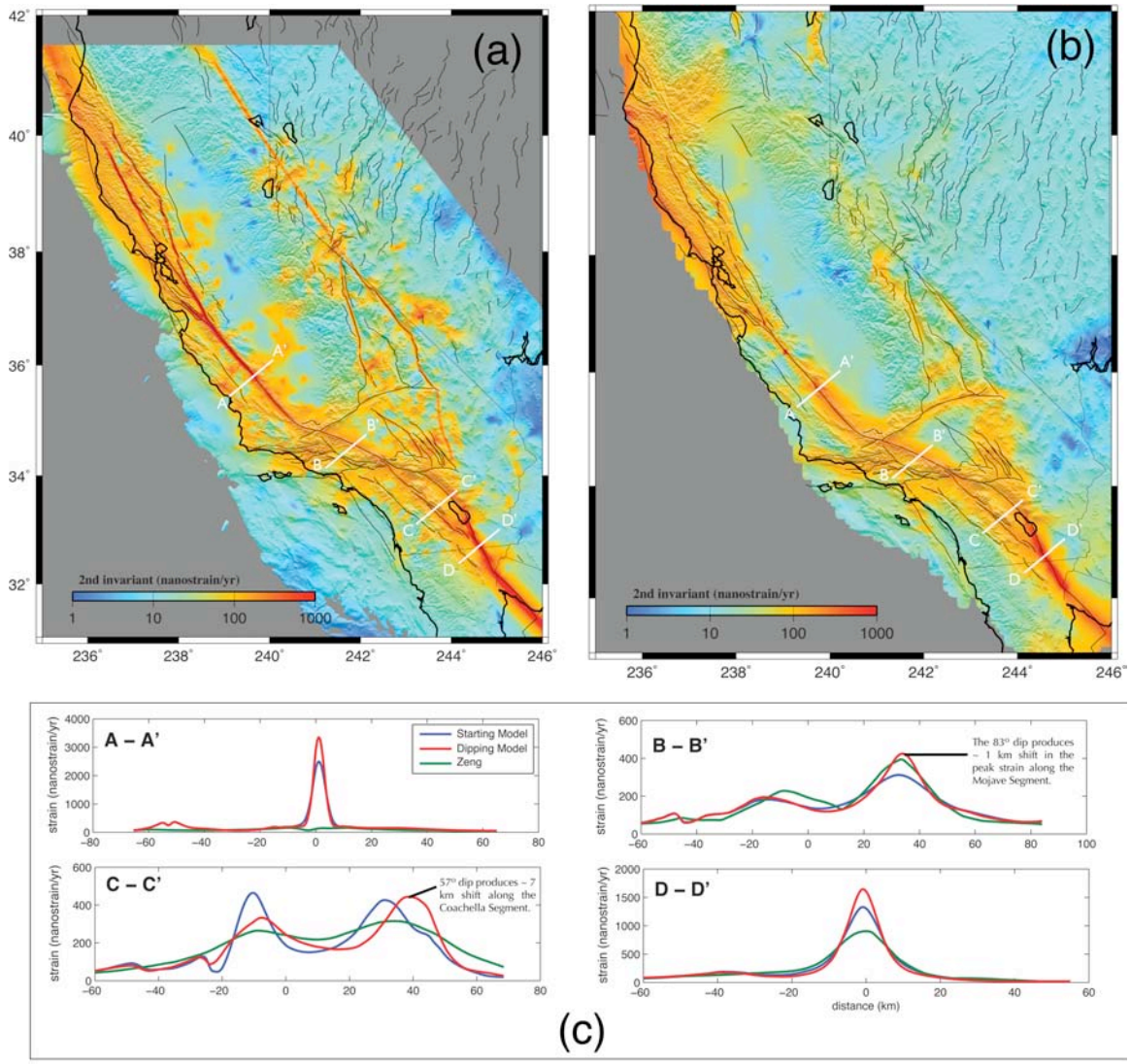


**Figure 3.** Strain rate comparison of Smith-Konter and Zeng models. (a) Strain rates derived from the Smith-Konter 3-D semi-analytic crustal deformation model (including dipping fault geometry) using optimized locking depth results to fit new PBO geodetic data. Model velocities were supplemented with an additional velocity model component developed by gridding the residuals to the GPS data using the GMT surface program with a tension of 0.35. White lines indicate profile locations of (c). (b) Strain rates calculated using Zeng model, which simulates the strain rate distribution for California and its neighbors analytically using the method of *Okada* [1992] (see text for additional details). White lines indicate profile locations of (c). (c) Strain rate profiles across the SAFS at four different locations marked in (a) and (b). For dipping faults in the Smith-Konter model, peak strain rates are horizontally shifted in the fault-perpendicular direction by a distance that scales as ~ $d$*tan(dip angle). Smith-Konter's "starting" model is represented by the blue line, Smith-Konter's optimized "dipping" model is represented by the red line, and Zeng's model is represented by the green line. Variations in strain rate magnitude between "Starting" and "Dipping" models are due to a change in locking depth.

## 4. OUTREACH ACTIVITIES PERFORMED DURING SCEC3

A significant component of SCEC3 funded projects emphasized Earth Science education and communication of pertinent and accessible earthquake information to the general public. Directly aimed at disseminating geoscience educational material to our local community, we worked closely with the UTEP Pathways to the Geosciences program to develop education content for our department's high school summer camp program. Smith-Konter participated in several summer sessions UTEP Pathways Summer Camp for high school students, where she lead students through a series of hands-on experiments and educational activities centered on plate tectonics.

We have been actively sharing relevant research material with the UTEP Cyber-ShARE Center and SIO Visualization Center. Both centers have been coordinating activities with us to catalog relevant images, animations, and interactive 3-D visualization scene files. With the recent opening of the UTEP Visualization Center, we have also be able to collaborate with the Center's interns and graduate students to develop interactive 3-D Fledermaus visualizations derived from our modeling efforts.

## 5. BIBLIOGRAPHY OF ALL PUBLICATIONS SUPPORTED BY SCEC3 FUNDS

Del Pardo, C., B. Smith-Konter, C. Kreemer, G. Blewitt, W. Hammond, and L. Serpa (2012 in revision), Interseismic deformation and stress evolution of the Death Valley Fault Zone, submitted to *Journal of Geophysical Research*, doi:10.1029/2011JB008552.

Smith-Konter, B., D.T. Sandwell, and P. Shearer (2011), Locking depths estimated from geodesy and seismology along the San Andreas Fault System: Implications for seismic moment release, *Journal of Geophysical Research*, 116, B06401, doi:10.1029/2010JB008117.

Smith-Konter, B., D.T. Sandwell, and M. Wei (2010), Integrating GPS and InSAR to resolve stressing rates of the SAF System, *EarthScope inSights*, Summer 2010.

Wei, M., D.T. Sandwell, and B. Smith-Konter (2010), Optimal combination of InSAR and GPS for measuring interseismic crustal deformation, *Journal of Advances in Space Research,* doi: 10.1016/j.asr.2010.03.013.

Smith-Konter, B. and D.T. Sandwell (2009), Stress evolution of the San Andreas Fault System: Recurrence interval versus locking depth, *Geophysical Research Letters*, 36, doi:10.1029/2009GL037235.